Fabrication of Artificial Nano Basement Membranes for Cell Compartmentalization in 3D Tissues

COMPASS

ENGINEERING LIFE GUIDED BY NATURE

This paper must be cited as: Zeng, J., Sasaki, N., Correia, C. R., Mano, J. F., & Matsusaki, M. Fabrication of Artificial Nanobasement Membranes for Cell Compartmentalization in 3D Tissues. *16*(24), 1907434. *Small*, (2020). https://doi.org/https://doi.org/10.1002/smll.201907434

Fabrication of Artificial Nano-Basement Membranes for Cell Compartmentalization in 3D Tissues

*Jinfeng Zeng, Naoko Sasaki, Clara R. Correia, João F. Mano and Michiya Matsusaki**

J. Zeng, Dr. N. Sasaki, Prof. M. Matsusaki

Division of Applied Chemistry, Graduate School of Engineering, Osaka University, Japan.

2-1 Yamadaoka, Suita, Osaka 565-0871, Japan.

E-mail: m-matsus@chem.eng.osaka-u.ac.jp

Dr. C. R. Correia, Prof. J. F. Mano

Department of Chemistry, CICECO-Aveiro Institute of Materials, University of Aveiro,

Campus Universitário de Santiago, 3810-193, Aveiro, Portugal.

Abstract

In recent decades, tissue engineering techniques have attracted much attention in the construction of three-dimensional (3D) tissues or organs. However, even though precise control of cell locations in 3D has been achieved, the organized cell locations were easily destroyed because of the cell migration during the cell culture period. In the human body, basement membranes (BMs) maintain the precise cell locations in 3D (compartmentalization). Constructing artificial BMs that mimic the structure and biofunctions of natural BMs remains a major challenge. Here, we report a nanometer-sized artificial BM through layer by layer assembly of collagen type IV (Col-IV) and laminin (LM), chosen because they are the main components of natural BMs. This multilayered Col-IV/LM nanofilm imitates natural BMs structure closely, showing controllable and similar components, thickness and fibrous network. The Col-IV/LM nanofilms had high cell adhesion properties and maintained the spreading morphology effectively. Furthermore, the barrier effect of preventing cell migration but permitting effective cell-cell crosstalk between fibroblasts and endothelial cells, demonstrates the ability of Col-IV/LM nanofilms for cell compartmentalization in 3D tissues, providing more reliable tissue models for evaluating drug efficacy, nanotoxicology, and implantation.

1. Introduction

The basement membrane (BM) is a specialized form of extracellular matrix (ECM) found adjacent to all cell monolayers.[1,2] It has been identified as a dense, continuous sheet-like structure with a thickness of 50-100 nm.[3] Collagen type IV (Col-IV) and laminin (LM) are the main components, which form two independent networks by self-assembly and the networks are cross-linked by other ECM proteins, such as nidogen, perlecan, and agrin.[3,4] The BMs not only provide structural support, but also regulate cell-cell contact cross BMs together with cell compartmentalization for maintaining complex tissue structures.[5] The successful construction of artificial BMs will contribute to advances in tissue engineering.

In the last decade, hydrogel scaffold[6,7] and non-scaffold techniques[8] have been extensively used for three-dimensional (3D) tissue construction. However, in many cases, the complex internal structures of these 3D tissue models are still limited and multiple types of cells are embedded randomly. Thus, it is still a huge challenge to replicate complex and well-organized tissues *in vitro*. Controlling patterned cells localization will be of great importance for the construction of complex compartmentalized 3D tissues.[9] Micropatterned cells co-culture systems have been used to enhance the control of spatial localization of multiple types of cell based on different levels of adhesiveness on the patterned substrates.[10,11] However, indirect guidance of cell patterning by patterned material adhesiveness on the substrate is unsuitable for 3D cells co-culture, with limitations in the control of resolution and cell position on existing cell layers. Ma[12] and Onoe[13] *et al.* reported the fabrication of anisotropic hydrogel microparticles by multi-fluidic electrostatic spraying technique and centrifuge-based microfluidic device respectively for efficient and scalable 3D cells culture. Even though these patterned hydrogel microparticles showed great potential for constructing size-controlled microtissues, cell migration was still not preventable without any substantial barriers. Furthermore, macroscopically, encapsulated cells were still in a random state, limiting the construction of compartmentalized 3D tissues. Until now, there has been only one

report by Takayama[14] *et al.* about customized cell-printing on a cell monolayer for 3D cells co-culture based on an optimized polymeric aqueous biphasic system. However, well-organized 3D tissues with cell compartmentalization are still unavailable.

In vivo, cells and ECM are hierarchically organized by BMs that divide tissues into compartments.[2] Considering the importance of BMs in tissue compartmentalization, the construction of artificial BMs will be useful for the development of functional organized tissue models.[15] Inspired by the ultra-thin, flexible, permeable, and fibrous structure, several attempts have been reported for patterned cells co-culture from simple polymer membranes[16,17] to complex ultrathin nanofilms[5,18–21]. However, due to the complex structure of natural BMs, these efforts still encountered obstacles to replicate such sophisticated structures and multifunctionality *in vitro*.[5] For example, the higher porosity and fibrous structure of electrospun scaffolds suggested that they would be the best candidate for producing BM-like membranes. These functional nanofiber meshes permitted bipolar cultivation of epithelial (endothelial) cells and mesenchymal cells, forming human primary alveolar-capillary barrier models[20,21], skin models[15] and so on. Although these nanofiber meshes showed similar barrier function and permeability, the biofunctions of BMs were not investigated in detail. However, BMs have been demonstrated to not only separate cells or tissues mechanically, but also regulate cell behaviors and promote cell "communications". Most of the electrospun fibers are limited to synthetic materials and micron thickness, in which the investigation of cell and materials interaction is limited.

Inspired by nature, biofunctional materials can be reconstructed following the design strategies of natural BMs. As one of the simplest but most useful methods, ECM proteins have been widely used to imitate natural ECM in cell-based assays.[8,22–25] In the same way, Matrigel, an extract of BMs from Engelbreth-Holm-Swarm (EHS) tumor, consists of almost the same components as natural BMs, which makes it the most BM-like natural matrix model.[25] Nevertheless, due to the tumorigenic origin and species difference, its safety has

been disputed. Fortunately, Col-IV and LM, the main components of BMs, are secreted by cells, and initiate intermolecular self-assembly, forming sheet-like structures.[4,26–28] BMs contain key biophysical and biochemical characteristics that are essential for cell attachment via the interactions between integrins and BMs proteins, especially Col IV and LM.[25] The Col-IV network contributes to the mechanical properties of BMs[29] and plays a critical role in the migration and adhesion of epithelial cells, which are the essential processes of re- epithelialization. LM is a highly biologically active molecule that plays essential roles in the regulation of cell adhesion, phenotyping, proliferation and differentiation.[23,25]

In this study, we fabricated an ultrathin nanofilm using Col-IV and LM to construct artificial BM with nanometer-sized thickness using layer by layer (LbL) assembly method.

Our group has been active in the study of LbL assembly for cell encapsulation and 3D tissues construction.[30–33] Recently, the feasibility of LbL assembly to control cell functions via modification on various substrates or cell encapsulation was summarized.[34] We also reported a bottom-up strategy through alternate deposition of fibronectin (FN)/gelatin (G) LbL nanofilm and fibroblasts layers to construct 3D tissue models, in which the FN/G nanofilms acted as nano-ECM for cell adhesion.[32] However, FN/G nanofilms are not suitable for cell compartmentalization, because cells can migrate cross the membrane easily and they are not the components of natural BMs. Here, we designed a Col-IV/LM multilayered nanofilm derived from the main components of BMs, which exhibited similar structures and biofunctions as natural BMs (Scheme 1). We characterized some of the necessary physicochemical and biological properties. Our findings demonstrate the barrier effect of (Col-IV/LM)5 nanofilms, preventing cell migration but permitting cell-cell communication, and provide a basis for the development of artificial BMs to construct compartmentalized 3D tissues in the future.

2. Results and Discussion

The preparation of nanometer-scale multilayered nanofilms was assessed using a quartz crystal microbalance (QCM) by the alternate deposition of Col-IV and LM. LM was demonstrated to bind preferentially to Col-IV over other collagens based on biologically specific recognition.[35] Figure 1 shows the results of LbL assembly of Col-IV and LM. In the Fourier Transform Infrared Spectroscopy (FTIR), for example, the amide I and II groups (νC=O:1663 cm^{-1} and δN-H: 1651 cm^{-1}) in Col-IV and LM monolayers were shown in (Col-IV/LM)5 and (Col-IV/LM)4-Col-IV nanofilms, but not in QCM ship, which confirm the successful adsorption of Col-IV and LM on the QCM chip surface (Figure S1). The LbLassembly process of polyelectrolyte based on electrostatic interaction is influenced by ionic strength because of the charge shielding effects.[36] Firstly, the effect of sodium chloride (NaCl) amount on LbL assembly of Col-IV and LM was analyzed (Figure 1a). As expected, frequency shift (Δf) and thickness clearly increased with the alternate deposition of Col-IV and LM onto a gold piezoelectric crystal without NaCl, confirming the interactions between Col-IV and LM. Unlike polyelectrolyte, the frequency shift and thickness of (Col-IV/LM)5 nanofilms decreased with the increase of NaCl concentration. This is probably because of the interactions between Col-IV and LM such as electrostatic interaction were weakened by the charge shielding effects. Meanwhile, spatial structure of proteins cannot be changed within a certain concentration range of NaCl. Thus, fewer Col-IV or LM molecules can be absorbed onto the previous layer which shows weaker interaction with more NaCl ions. From this basis, Tris-HCl buffer solution without NaCl was used for further preparations of (Col-IV/LM)5 nanofilms. The thickness of (Col-IV/LM)5 nanofilms can be adjusted in the range of 5-80 nm by controlling the concentration of Col-IV and LM (Figure 1b) making them similar to natural BMs that are around 50 nm thickness.[3] Due to the strong interaction between Col-IV and LM and advantages of the LbL assembly technique, 5 nm of nanofilms can be obtained from even the lowest concentration, 4 μg/mL (Figure 1b, Figure S2). Thus, (Col-IV/LM)5 nanofilms are appropriate for the construction of artificial BMs with various

thicknesses in different 3D tissue models. The thickness of (Col-IV/LM)5 nanofilms increased linearly (1,000 μg/mL, R^2=0.9998) for each assembly cycle with a steady increase at around 13.5 nm (Figure 1c). Taken together, these data indicate the potential of(Col-IV/LM)5 nanofilms used for the construction of artificial BMs. Next, the weight remaining percentage of (Col-IV/LM)5 nanofilms at various thicknesses in PBS (pH=7.4) buffer solution was evaluated at 37 °C by analysing frequency change of QCM, which has been reported in our previous paper[38]. All the nanofilms showed good stability in PBS for up to 7 days, although they exhibited a weight increase in the first 5 hours because of the swelling effect (Figure 1d). Even though the amount of nanofilms at 1,000 μg/mL showed a sustained decrease, the remaining weight were still around 80% after 7 days incubation (Figure S3).

Figure 2 shows the enzymatic degradation behaviors of (Col-IV/LM)5 nanofilms in collagenase type IV/PBS solution (pH=7.4, 37 °C). Both of the 40 (26 nm) and 1,000 μg/mL (75 nm) nanofilms degraded rapidly and the weight remaining percentage decreased below 10% after 180 min, but kept stable in PBS solution without enzyme (Figture 1d). Good stability and biodegradability indicated that (Col-IV/LM)5 nanofilms are suitable for tissue engineering.

Since both endothelial and mesenchymal cells are co-localized nearby with an indirect crosstalk and adhere well to the natural BMs, the cell adhesion properties of these two types of cells were evaluated on the obtained artificial BMs. Surface wettability of substrate is one of the most critical factors for cell adhesion behaviors. In order to analyze the cell adhesion properties of (Col-IV/LM)5 nanofilms, the nanofilms were coated on the surface of a polystyrene (PS) substrate that is hydrophobic. Normal Human Dermal Fibroblasts (NHDF) and Human Umbilical Vein Endothelial Cell (HUVEC) were seeded on the nanofilms surface, as shown in Figure 3a. Bare PS substrate served as a negative control, which is not suitable for fibroblasts and endothelial cells adhesion. Meanwhile, the tissue culture dish is also made from polystyrene, but treated with plasma to be applicable for tissue culture and referred to as

TCPS, served as a positive control. Firstly, water contact angles of various substrates were measured, as shown in Figure 3b. Compared with TCPS, the PS substrate is more hydrophobic. Significant differences were observed between PS substrate and Col-IV/LM nanofilms. After layer by layer assembly of Col-IV/LM nanofilms on QCM chips, the water contact angle decreased greatly. There was, however, no significant difference between (Col- IV/LM)$_5$ and (Col-IV/LM)$_4$-Col-IV nanofilms maybe because of the exposure of both Col-IV and LM on the surface. Live/Dead cells imaging assessed the viability of (Col-IV/LM)$_5$ nanofilms (Figure 3c). Compared to TCPS, there were 97% of viability at (Col-IV/LM)$_1$, 94% at (Col-IV/LM)$_3$ and 110% at (Col-IV/LM)$_5$, indicating the excellent viability of Col-IV/LM nanofilms even with only one bilayer (Figure S4). When cells were cultured for one hour on the bare PS substrate, few cells could attach to the substrate and all the cells presented a round shape morphology. However, both NHDF and HUVEC adhered well to Col-IV/LM nanofilms even with only one bilayer. More than 55% of NHDF and 60% of HUVEC adhered to (Col-IV/LM)$_5$ nanofilms after one hour of incubation, which showed even better adhesion properties than the TCPS substrate with 31% adhesion percentage of NHDF and 20% of HUVEC (Figure 3e, S5). Furthermore, after 24 hours incubation, 135% of NHDF and 129% of HUVEC adhered well to (Col-IV/LM)$_5$ nanofilms, and displayed their normal cobblestone-like and fiber-like morphologies. However, less than 40% of cells adhered to the bare PS substrate, and the poorly adhered NHDF and HUVEC showed strong aggregation (Figure 3d, S6). These results demonstrated the good cell adhesion properties of Col-IV/LM nanofilms because the Col-IV and LM can not only increase the hydrophilicity of the PS substate, but also provide sites for cell adhesion proteins, such as integrin. These cell adhesion properties satisfied the requirements for artificial BMs, indicating the possibility that Col-IV/LM nanofilms could be employed as artificial BMs.

Natural BMs play an important role in the separation of different cells and keeping compartmentalization of various tissues or organs. Moreover, BMs are closely associated with

cancer cells metastasis and invasion. Therefore, the cell separation property is one of the most critical factors, which is depicted in Figure 4. The transwell migration assay is usually used to analyze cell invasion ability or response to some chemotactic factors[39]. Here, $(Col\text{-}IV/LM)_5$ nanofilms were coated onto a transwell insert membrane who acted as a control group to compare the barrier effect of $(Col\text{-}IV/LM)_5$ nanofilms preventing cell migration (Figure 4a). HUVEC, which possess a stronger migration ability compared to NHDF, were used to test the cell separation effect of $(Col\text{-}IV/LM)_5$ nanofilms. For the bare insert membrane (3.0 μm of pore), HUVEC migrated easily to the other side through the pores. Migrated cells could be observed after 6 hours incubation (Figure S7), and the migrated cell number percentage increased from 9% to 72% after 48 hours incubation (Figure 4c, d). HUVEC migration behavior through the insert membrane was also confirmed by H&E staining (Figure S8), where HUVEC could be observed on both sides of the insert membrane, forming a "sandwich" structure. Compared with the bare insert membrane, $(Col\text{-}IV/LM)_5$ nanofilms at 40 μg/mL could prevent a small amount of cell migration in 12 hours, but there was no significant prevention effect after 12 hours. This maybe because of its lack of thickness at only 26 nm and enzymatic degradation by the cells. We assumed that a much stronger barrier effect would be exhibited with thicker nanofilms. $(Col\text{-}IV/LM)_5$ nanofilms at 75 nm obtained from 1,000 μg/mL were measured under the same experimental condition. These thicker nanofilms prevented cell migration completely for up to 8 hours, and showed very good separation ability for up to 48 hours, when less than 20% of cells showed migration. Based on the preceding analysis, there is plenty of potential for (Col-IV/LM)5 nanofilms with suitable thickness to prevent cell migration and separate different cells or tissues, thus mimicking natural BMs.

In addition, natural BMs distribute between epithelial (endothelial) cells and connective tissues *in vivo*. To further assess the barrier effect of Col-IV/LM nanofilms between different cells, $(Col\text{-}IV/LM)_5$ nanofilm at 75 nm thickness was placed between NHDF layers and an

HUVEC monolayer, which mimics the structure of natural tissues (Figure 5a). The location of (Col-IV/LM)5 nanofilms was confirmed by the cross-sectional confocal laser scanning microscopy (CLSM) (Figure 5b). (Col-IV/LM)5 nanofilms in green were distributed between the HUVEC monolayer (CD31 stained in blue) and the NHDF layers (cell tracker^{TM} deep red). Figure 5d shows the morphology of (Col-IV/LM)5 nanofilms at 26 nm, in which Col-IV was conjugated with FAM in green. These network structures can not only support adhered cells, but also allow the transport of small signal molecules for heterocellular crosstalk, which is similar to natural BMs. At first, HUVEC monolayer was localized hierarchically on the surface of NHDF layers (Figure 5c), but migrated into NHDF layers quickly within two days (Figure S9). However, with the barrier effect of $(Col\text{-}IV/LM)_5$ nanofilms between HUVEC and NHDF, the migration of HUVEC was prevented effectively. Without any barriers, HUVEC migrated deeply to over half the depth of NHDF layers in the first 24 hours of incubation and even reached to the bottom, forming a random cells mixture on the fourth day (Figure 5e,f,g). But under the barrier effect of $(Col\text{-}IV/LM)_5$ nanofilms, after 2 days incubation, HUVEC and NHDF still kept their layered and organized structure. Even on the third day, the depth of HUVEC migration through NHDF layers was still less than 50%, indicating the successful barrier effect of $(Col\text{-}IV/LM)_5$ nanofilms. After 4 days incubation, however, HUVEC migrated almost to the bottom. The $(Col\text{-}IV/LM)_5$ nanofilms may have been partialy degraded by some enzyme secreted by fibroblasts[40]. Despite this, the migrated cell number was still less than that without $(Col\text{-}IV/LM)_5$ nanofilms (Figure 5h), indicating their effective barrier function.

In vivo, cell compartmentlizations are supported by natural BMs due to the barrier effects. However, natural BMs are not completely enclosed sheet-like nanofilm, but densely fibrous network with pores that allow the transport of signal molecules, improving the cross-talk between adjacent cells.[5] Therefore, the transport of signal molecules secreted by cells through artificial BMs is another important factor for the construction of compartmentalized

3D tissues. We analyzed tight juntion proteins expression of HUVEC co-cultured with NHDF by RT-qPCR, and compared the gene expression value with only HUVEC culture by normalization using VE-cadherin gene expression because this gene is expressed only in HUVEC, but not NHDF. Intercellular tight junction proteins including ZO-1, occludin-1, claudin-4 are crucial for the formation of endothelial barriers, as they regulate cell adhesion and migration.[41] And basic fibroblast growth factor secreted by NHDF was demonstrated to promote endothelial cell-primed angiogenesis.[42] Co-culture with NHDF, the expression of tight junction proteins and adhesion molecules of HUVEC will be improved. In Figure 6, compared with only HUVEC culture, relative RNA expression values of tight junction proteins were significantly higher. Especially for claudin-4, the expression value was more than 10 times higher than only HUVEC culture, indicating that the existence of NHDF improved HUVEC cell-cell contact and differentiation. There were no significant differences between co-culture of NHDF and HUVEC without or with the separation of $(Col\text{-}IV/LM)_5$ nanofilms, demonstrating that $(Col\text{-}IV/LM)_5$ nanofilms showed no suppression effect to the cross-talk between NHDF and HUVEC with the barrier effect of artificial BMs. These results clearly demonstrated molecules transport effect of the $(Col\text{-}IV/LM)_5$ nanofilms same as natural BMs, because of the fibrous networks structure of (Figure 5d).

3. Conclusion and Outlook

Our results demonstrate the ability of artificial BMs based on LbL nanofilms to imitate the structure and biofunctions of natural BMs. Simple operation and materials-versatility of the LbL assembly method enable the fabrication of nanometer-sized films with controllable components and thickness. The obtained multilayered Col-IV/LM nanofilms showed adjustable components, thickness and fibrous networks that are all similar to natural BMs. High cell adhesion properties were also demonstrated. These multilayered Col-IV/LM nanofilms permitted compartmentalized co-culture of fibroblasts and endothelial cells resembling as a barrier, but allowed cell-cell cross-talk even with the separation effect,

indicating the potential application of the LbL assembly method for artificial BMs, which could be used for the construction of compartmentalized 3D tissues. Furthermore, our group have reported a rapid and automatic manipulation of FN/G LbL nanofilms by the incorporation of the LbL assembly method and 3D printing.[41] The compatibility of the LbL assembly method with bioprinting will increase the complexity of LbL nanofilms. Inspired by this, we are still working on the preparation of custom-shaped artificial BMs. After that, compartmentalized 3D tissues with various structures will be possible through user-defined artificial BMs and patterned cells co-culture.

4. Experimental Section

Materials: Collagen type IV (Col-IV) was purchased from Sigma-Aldrich (C7521, Missouri, USA). Laminin-111 (LM) was purchased from Corning (354259, New York, USA). Normal human dermal fibroblast cells (NHDF, CC-2509), and Human umbilical vein endothelial cells (HUVEC, C2517A), were got from Lonza (Basel, Switzerland). GFP expressed Human umbilical vein endothelial cells (GFP-HUVEC) were purchased from Argio-Proteomie (Massachusetts, USA). Collagenase type IV was purchased from Gibco BRL, Life Technologies (Rockville, Maryland, USA). Crystal violet hydrate was purchased from TCI (548-62-9, Tokyo, Japan). Collagen type IV, FAM conjugated was purchased from AnaSpec (AS-85112, California, USA), and Laminin (Red fluorescent, rhodamine) was purchased from Cytoskeleton (LMN01-A, Colorado, USA). Cell tracker™ Deep red, PureLink RNA Micro Kit and the pacific blue™ of goat anti-mouse IgG were purchased from Invitrogen (California, USA). Monoclonal mouse anti-human CD31 antibody was purchased from Dako (M0823, Glostrup, Denmark). An AT-cut quartz crystal (9 mm diameter) with a parent frequency of 9 MHz and a frequency counter (model 53131 A) were purchased from USI (Fukuoka, Japan). ReverTra Ace® qPCR RT Master Mix and Thunderbird® SYBR® qPCR Mix were purchased from Toyobo (Osaka, Japan).

(Col-IV/LM)5 multilayered nanofilm preparation and characterization: The quantitative analysis of LbL assembly was performed using a quartz crystal microbalance (QCM) as our previously reported protocols.[30,31] At first, the QCM chip was treated by Piranha solution (H_2SO_4/40% H_2O_2 aqueous solution=3:1 in volume) twice. Following the cleaning step, the QCM chip was alternately immersed into Col-IV (40 μg/mL) and LM (40 μg/mL)/Tris-HCl buffer solution (50 mM, pH=7.4) for 15 min at 37 °C. Between each step, the QCM chip was rinsed with 1 mM Tris-HCl buffer solution (pH=7.4), and then dried under N_2 gas. The alternate steps were repeated until 5 bilayers, the nanofilm was denoted as $(Col\text{-}IV/LM)_5$. For each step, frequency shift (ΔF) was recorded, and the amount (Δm) of deposition was obtained by calculating according to the Sauerbrey equation: $-\Delta F/Hz=1.15\ \Delta m/ng$.[44] After further calculation according to the deposited amount and assumed nanofilm density of proteins and polyelectrolytes at 1.3 and 1.2 g/cm^3,[45] respectively, the thickness of the resultant $(Col\text{-}IV/LM)_5$ nanofilms was obtained. In the same way, LbL assembly of Col-IV and LM solution at 4, 8, 80, 400 and 1,000 μg/mL were also performed and the effects of NaCl on LbL assembly were analyzed by adding various amounts of NaCl into Tris-HCl buffer solution (0, 0.15, 1 mol/L respectively).

Characterization of $(Col\text{-}IV/LM)_5$ nanofilms: The stability of $(Col\text{-}IV/LM)_5$ nanofilms was measured by immersing samples coated onto the QCM chips into PBS solution (pH=7.4) at 37 °C for 7 days. Frequency shifts of the QCM chips were recorded at intervals. The degradation of (Col-IV/LM)5 nanofilms was analyzed by immersing them into a collagenase-IV/PBS solution (100 U/mL) at 37 °C. The weight of the remaining nanofilms was measured using QCM. The surface wettability of (Col-IV/LM)5 nanofilms was analyzed through the contact angles between water and the surface of the samples. Contact angles of (Col-IV/LM)5 nanofilms were evaluated by Drop Master (Kyowa Interface Science, Saitama, Japan).

Cell culture: NHDF (Passage: 6-8) were cultured with DMEM containing 10% FBS and 1%

penicillin/streptomycin in 5% CO_2 at 37 °C. HUVEC (Passage: less than 8-10) were cultured in EGM-2.

Cell tracker staining: Briefly, Cell Tracker™ Deep Red was dissolved in dimethyl sulfoxide (DMSO) at 10 mM, then diluted into FBS-free medium at 1:1000 (v:v). Pre-cultured cells were rinsed with PBS three times and exposed to the diluted dye for 40 min at 37 °C. Next, the medium with Cell Tracker was aspirated, and cells were washed with PBS three times. Cells were incubated with DMEM at 37 °C for at least 24 hours before being detached.

Immunofluorescence staining: After incubation, samples were washed with PBS three times and fixed by 4% paraformaldehyde (PFA) for 15 min at room temperature. After washing with PBS three times, 0.2% Triton-X 100 was incubated with cells for enhancing antibody permeability for 30 min at room temperature. Next, after washing with PBS three times, 1% BSA/PBS solution was added at room temperature for 30 min in order to block the unspecific staining of the antibody. The cells were then washed with PBS three times and incubated with CD31 (primary antibody, diluted 100 times in 1% BSA/PBS solution) at 4 °C, overnight. After a further three times washes with PBS, Pacific Blue™ (secondary antibody, anti-mouse, diluted 100 times in 1% BSA/PBS solution) was added and samples were incubated at room temperature for 2 hours. Fluorescence images were observed with confocal laser scanning microscopy (CLSM, FV3000, Olympus, Japan).

Histology staining: Samples were fixed in 4 % PFA for 15 min at room temperature, washed with PBS three times, and then sent to the Applied Research Company for paraffin embedding. Sectional samples were stained with hematoxylin and eosin (H&E) and CD31. Brightfield images were captured using an FL Evos Auto microscope (Thermo Fisher Scientific, MA, USA).

Cell adhesion: 6-well polystyrene plates with or without tissue culture treatment were used for cell culture substrate, denoted as TCPS and PS, respectively. As for LbL assembly using QCM, 2 mL of Col-IV (40 μg/mL) and LM (40 μg/mL)/Tris-HCl buffer solution (50 mM,

pH=7.4) were alternately added into the 6-well plate, incubated at 37 °C for 15 min, followed by a rinsing step between each protein deposition by 1mM of Tris-HCl solution. The alternate steps were repeated until the desired bilayer numbers were reached. The multilayered nanofilms were washed with PBS three times. 1.0×10^4 of NHDF and HUVEC in 2 mL medium were seeded onto the nanofilms, respectively. After one- and 24-hours of incubation, the culture medium was removed and samples were washed with PBS three times to remove nonadherent cells. Cell morphology was observed using an FL EVOS Auto microscope (Thermo Fisher, USA). Cell number was counted by trypan blue staining.

Cell Viability: The viability of NHDF with (Col-IV/LM)5 nanofilm was performed using a Live/Dead® viability assay kit and WST-8 kit assay. (Col-IV/LM)5 nanofilms were coated into a cell culture plate by LbL assembly and were washed with PBS three times. For Live/Dead® viability assay kit, 1 mL of 1.0×10^5 NHDF were seeded in each well (24-well plate) and then incubated at 37 °C for 24 hours. After a further washing with PBS, 300 μL of PBS solution containing Calcein AM and EthD-1/PBS (2 μmol/L) was added into each well, followed by incubation at 37 °C for 45 min in the dark. After incubation, the nanofilms were washed with PBS three times. Images were obtained using a confocal laser scanning microscope (FV3000). ImageJ software was used for the analysis of the projections, calculating the percentage of each staining (1280×1280 μm, n=3). For WST-8 kit assay, 100 μL of 1.0×10^4 NHDF were cultured in 96-well plate at 37 °C for 24 hours. After a further washing with PBS, 100 μL of cell count reagent SF/DMEM (1:9, without phenol red) was added to each well. The cells were incubation for another 3 hours at 37 °C. And then transferring the supernatant to a new well, the absorbance of supernatant at 450/600 nm was measured by microplate reader.

Cell compartmentalization: The barrier effect of (Col-IV/LM)5 nanofilms was analyzed by the "scaffold" and "sandwich" methods. For the "scaffold" method, a 24-well insert with a 3.0 μm pore size served as a "scaffold" and (Col-IV/LM)5 nanofilms (40 μg/mL and 1,000 μg/mL,

respectively) were deposited onto the insert membrane. 300 μL of 2.0×10^5 HUVEC were seeded in each insert and 1 mL of medium was added outside. After incubation at 37 °C for 6, 8 12, 24 and 48 hours, part of the cells migrated to the other side of insert. After washing with PBS three times, un-migrated cells inside the insert were completely removed by cotton swabs and migrated cells were stained with crystal violet/PBS solution (1.0 mg/mL) for 15 min and then washed with PBS three times. The samples were then examined by phase contrast microscope. ImageJ software was used for the analysis of migrated cell number and coverage ratio. For the "sandwich" method, (Col-IV/LM)5 nanofilm (1,000 μg/mL) was deposited between NHDF layers (1.0×10^6) and a GFP-HUVEC (1.0×10^5) monolayer, forming a "sandwich" structure which is similar to the structure of natural tissue. First, 300 μL of 1.0×10^6 NHDF were seeded into a 24-well insert which was incubated into LM (40 μg/mL)/Tris-HCl solution (50 mM, pH=7.4) at 37 °C for 2 hours for cell adhesion. 1 mL of DMEM was added outside and the sample was incubated at 37 °C for 24 hours. After washing with PBS, Col-IV and LM/Tris-HCl solution were alternately added into the insert, forming (Col-IV/LM)5 nanofilms at the surface of NHDF layers. Following seeding with 1.0×10^5 HUVEC, cells were incubated at 37 °C. The migration of HUVEC after 1, 2, 3 and 4 days was observed by confocal laser scanning microscopy (FV3000). Images were digitized using Imaris software (ver. 9.2.1, Oxford Instruments) and migrated cell number and depth were calculated using ImageJ.

Gene expression: 1.0×10^6 NHDF were seeded into a 6-well insert and incubated at 37 °Cfor 24 hours for NHDF adhesion completely. After washing with PBS, Col-IV and LM/Tris-HCl solution (1000 μg/mL) were alternately added into the insert, forming (Col-IV/LM)5nanofilms at the surface of NHDF layers. Following seeding with 1.0×10^6 HUVEC, cells were incubated at 37 °C for 3 days, with medium changes every day. Gene expression was analyzed using real-time quantitative polymerase chain reaction (RT-qPCR).

After 3 days incubation, all samples were washed with PBS. RNA extraction was carried out using PureLink RNA Micro Kit following strictly the manufacturer instructions. RNA content of each sample was measured by Nanodrop™ spectrometer (N1000, Thermo Fisher Scientific). ReverTra Ace® qPCR RT Master Mix was used for reverse transcription to synthesize high quality cDNAs for RT-qPCR. Thunderbird® SYBR® qPCR Mix was employed to initiate and amplify the cDNA. The cDNA synthesis and RT-qPCR reactions were conducted using the StepOnePlus Real-Time PCR System (Thermo Fisher Scientific). After preliminary trials, PPIA was employed as the house keeping gene. Results were moreover normalized by VE-cadherin expression.

Supporting Information

Supporting Information is available from the Wiley Online Library or from the author.

Acknowledgements

The authors acknowledge financial support by Grant-in-Aid for Scientific Research (B) (17H02099) and Bilateral Joint Research Projects of the JSPS and the AMED Grant (JP18be0304207). The authors are also grateful for the financial support of the European Research Council for project ATLAS (grant agreement ERC-2014-ADG-669858), and the project CICECO-Aveiro Institute of Materials, FCT Ref. UID/CTM/50011/2019, supported by national funds through the FCT/MCTES.

Conflict of Interest

The authors declare no conflict of interest.

Received: ((will be filled in by the editorial staff))

Revised: ((will be filled in by the editorial staff))

Published online: ((will be filled in by the editorial staff))

References

[1] J. C. Schittny, P. D. Yurchenco, *Curr. Opin. Cell Biol.* **1989**, *1*, 983.

[2] M. P. M, *Crit. Rev. Biochem. Mol. Biol.* **1992**, *27*, 93.

[3] E. Hohenester, P. D. Yurchenco, *Cell Adhes. Migr.* **2013**, *7*, 56.

[4] R. Kalluri, *Nat. Rev. Cancer* **2003**, *3*, 422.

[5] G. Perry, W. Xiao, G. I. Welsh, A. W. Perriman, R. Lennon, *Integr. Biol.* **2018**, *10*, 680.

[6] C.Y. Liaw, S. Ji, M. Guvendiren, *Adv. Healthcare Mater.* **2018**, *7*, 1701165.

[7] M. Matsusaki, H. Yoshida, M. Akashi, *Biomaterials* **2007**, *28*, 2729.

[8] M. Matsusaki, C. P. Case, M. Akashi, *Adv. Drug Delivery Rev.* **2014**, *74*, 95.

[9] C.R.Correia, S.Nadine, J.F.Mano. Adv. Funct. Mater. 2019, DOI:10.1002/adfm.201908061. Accepted.

[10] P.O. Strale, A. Azioune, G. Bugnicourt, Y. Lecomte, M. Chahid, V. Studer, *Adv. Mater.* **2016**, *28*, 2024.

[11] R. Singhvi, A. Kumar, G. Lopez, G. Stephanopoulos, D. Wang, G. Whitesides, D. Ingber, *Science* **1994**, *264*, 696.

[12] Y.C. Lu, W. Song, D. An, B. J. Kim, R. Schwartz, M. Wu, M. Ma, *J. Mater. Chem. B* **2015**, *3*, 353.

[13] S. Yoshida, M. Takinoue, H. Onoe, *Adv. Healthcare Mater.* **2017**, *6*, 1601463.

[14] H. Tavana, B. Mosadegh, S. Takayama, *Adv. Mater.* **2010**, *22*, 2628.

[15] A. Rossi, L. Wistlich, K.H. Heffels, H. Walles, J. Groll, *Adv. Healthcare Mater.* **2016**, *5*, 1939.

[16] S. Suzuki, K. Nishiwaki, S. Takeoka, T. Fujie, *Adv. Mater. Technol.* **2016**, *1*, 1600064.

[17] H. J. Kim, D. Huh, G. Hamilton, D. E. Ingber, *Lab Chip* **2012**, *12*, 2165.

[18] R. N. Palchesko, J. L. Funderburgh, A. W. Feinberg, *Adv. Healthcare Mater.* **2016**, *5*, 2942.

[19] M. J. Mondrinos, Y.S. Yi, N.K. Wu, X. Ding, D. Huh, *Lab Chip* **2017**, *17*, 3146.

[20] E. Dohle, S. Singh, A. Nishigushi, T. Fischer, M. Wessling, M. Möller, R. Sader, J. Kasper, S. Ghanaati, C. J. Kirkpatrick, *Tissue Eng., Part C* **2018**, *24*, 495.

[21] A. Nishiguchi, S. Singh, M. Wessling, C. J. Kirkpatrick, M. Möller, *Biomacromolecules* **2017**, *18*, 719.

[22] F. Louis, S. Kitano, J. F. Mano, M. Matsusaki, *Acta Biomater.* **2019**, *84*, 194.

[23] A. E. Stanton, X. Tong, F. Yang, *Acta Biomater.* **2019**, *96*, 310.

[24] H. Nakatsuji, M. Matsusaki, *ACS Biomater. Sci. Eng.* **2019**, acsbiomaterials.9b00090.

[25] R. Cruz-Acuña, A. J. García, *Matrix Biology* **2017**, *57–58*, 324.

[26] P. D. Yurchenco, H. Furthmayr, *Biochemistry* **1984**, *23*, 1839.

[27] P. D. Yurchenco, J. C. Schittny, *The FASEB Journal* **1990**, *4*, 1577.

[28] T. Bhuvanesh, R. Machatschek, L. Lysyakova, K. Kratz, B. Schulz, N. Ma, A. Lendlein, *Biomed. Mater.* **2019**, *14*, 024101.

[29] G. Bhave, S. Colon, N. Ferrell, *Am. J. Physiol. Renal. Physiol.* **2017**, *313*, F596.

[30] A. Nishiguchi, H. Yoshida, M. Matsusaki, M. Akashi, *Adv. Mater.* **2011**, *23*, 3506.

[31] K. Kadowaki, M. Matsusaki, M. Akashi, *Langmuir* **2010**, *26*, 5670.

[32] M. Matsusaki, K. Kadowaki, Y. Nakahara, M. Akashi, *Angew. Chem., Int. Ed.* **2007**, *46*, 4689.

[33] M. Matsusaki, H. Ajiro, T. Kida, T. Serizawa, M. Akashi, *Adv. Mater.* **2012**, *24*, 454.

[34] J. Zeng, M. Matsusaki, *Polym. Chem.* **2019**, *10*, 2960.

[35] R. W. N. Nugroho, R. Harjumäki, X. Zhang, Y. R. Lou, M. Yliperttula, J. J. Valle Delgado, M. Österberg, *Colloids and Surfaces B: Biointerfaces* **2019**, *173*, 571.

[36] J.T. O'Neal, E. Y. Dai, Y. Zhang, K. B. Clark, K. G. Wilcox, I. M. George, N. E. Ramasamy, D. Enriquez, P. Batys, M. Sammalkorpi, J. L. Lutkenhaus, *Langmuir* **2018**, *34*, 999.

[37] D. Woodley, C. Rao, J. Hassell, L. Liotta, G. Martin, H. Kleinman, *Biochimica et Biophysica Acta (BBA) - General Subjects* **1983**, *761*, 278.

[38] Y. Nakahara, M. Matsusaki, M. Akashi, *Journal of biomaterials science. Polymer edition* **2007**, *18*, 1565.

[39] S. Iwai, S. Kishimoto, Y. Amano, A. Nishiguchi, M. Matsusaki, A. Takeshita, M. Akashi, *J. Biomed. Mater. Res.* **2019**, *107*, 292.

[40] D. Lindner, C. Zietsch, P. M. Becher, K. Schulze, H.-P. Schultheiss, C. Tschöpe, D. Westermann, *Biochem. Res. Int.* **2012**, *2012*, 1.

[41] M. Matsusaki, K. Sakaue, K. Kadowaki, M. Akashi, *Adv. Healthcare Mater.* **2013**, *2*, 534.

[42] G. Bazzoni, E. Dejana, *Physiol. Rev.*, **2004**, *84*, 869.

[43] M. Presta, P. Dell'Era, S. Mitola, E. Moroni, R. Ronca, M. Rusnati, *Cytokine Growth Factor Rev.* **2005**, *16*, 159.

[44] G. Z. Sauerbrey, *Phys.* **1959**, *155*, 206.

[45] Y. Lvov, K. Ariga, I. Ichinose, T. Kunitake, *J. Am. Chem. Soc.* **1995**, *117*, 6117.

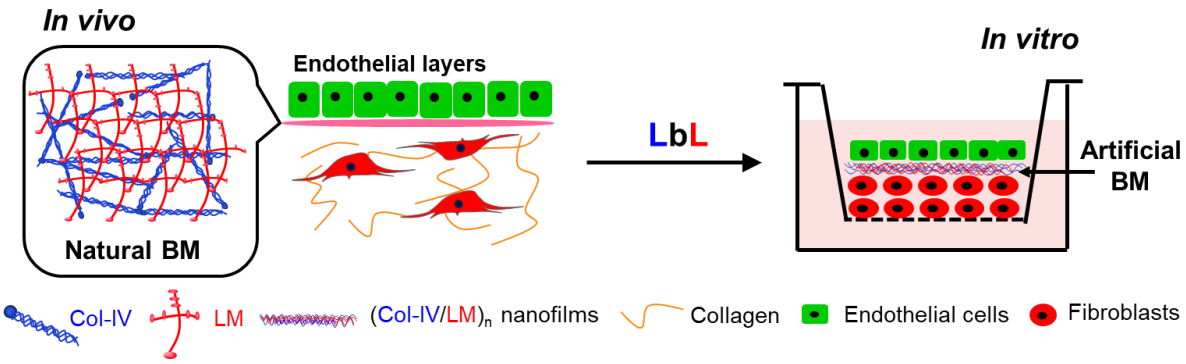

Scheme 1. Schematic illustration of fabrication of artificial basement membranes (BMs) through the layer by layer assembly process of Col-IV and LM derived from natural BMs.

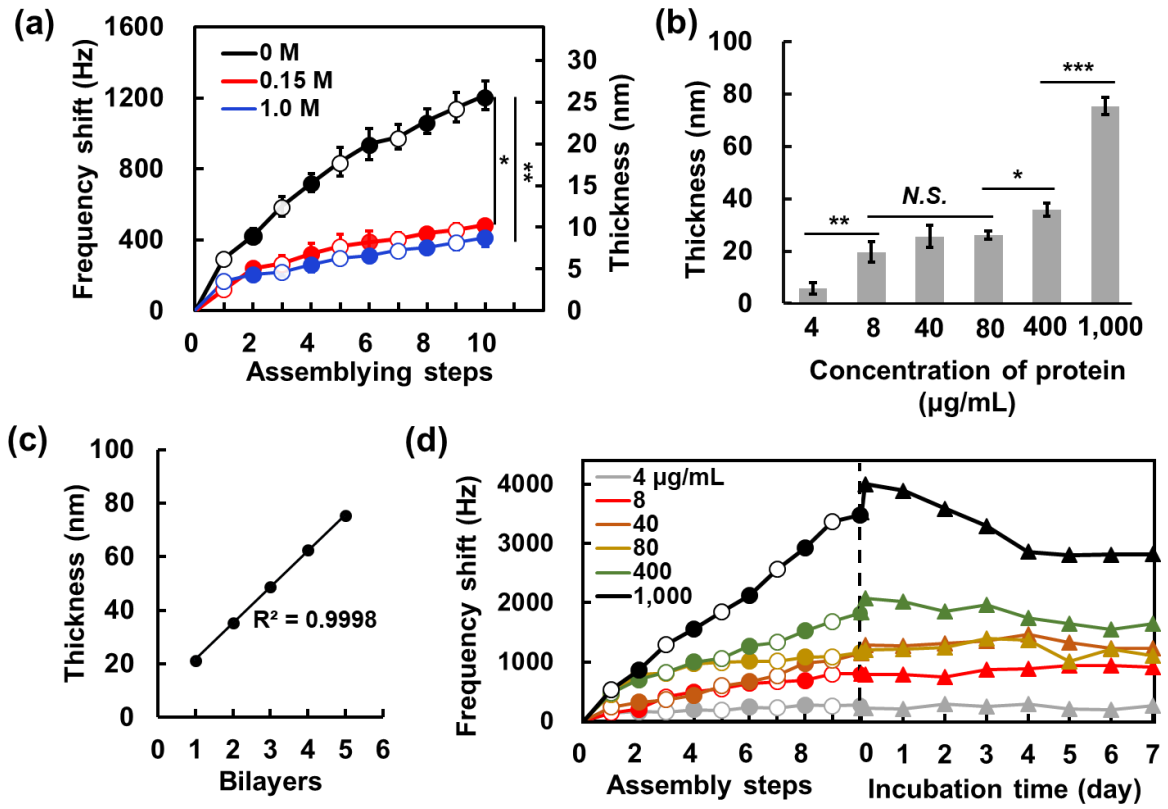

Figure 1. Buildup of Col-IV/LM multilayered ultrathin nanofilms onto QCM chips. (a) Frequency shift and thickness increase of Col-IV (□) and LM (●) at 37 °C in 50 mM Tris-HCl buffer solution (pH=7.4) with different concentrations of NaCl. n=3. (b) Thickness of (Col-IV/LM)5 nanofilms obtained from Col-IV and LM solutions at various concentrations. n=3. (c) Cumulative thickness evolution of Col-IV/LM multilayered nanofilms as a function of the number of deposition layers. The concentrations of Col-IV and LM solutions were 1,000 μg/mL, respectively. (d) Left: Frequency shifts of the QCM stepwise assembly of Col-IV/LM nanofilms at 37 °C in 50 mM Tris-HCl buffer solution (pH=7.4) with various concentrations of proteins. Right: Stability of different thicknesses of (Col-IV/LM)5 nanofilms in PBS buffer solution (pH=7.4) at 37 °C analyzed by QCM. *p<0.05, **p<0.01, ***p<0.001.

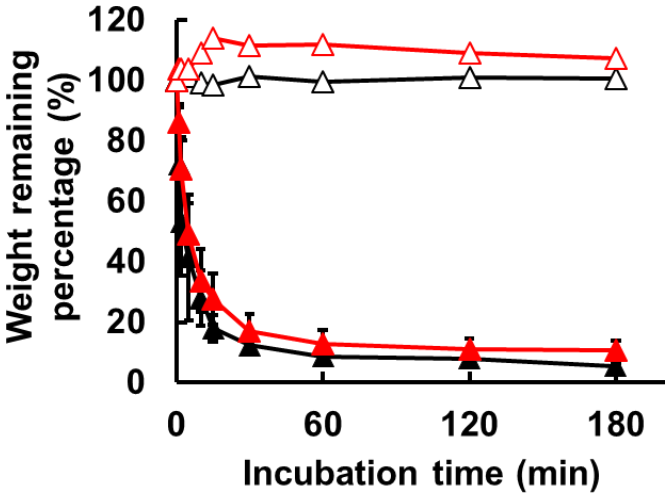

Figure 2. Enzymatic degradation of $(Col\text{-}IV/LM)_5$ nanofilms with 26 nm obtained from 40 μg/mL (black) and nanofilms with 75 nm obtained from 1,000 μg/mL (red) in PBS buffer solution with (▲) or without (Δ) collagenase-IV (100 U/mL, pH=7.4) at 37 °C analyzed by QCM.

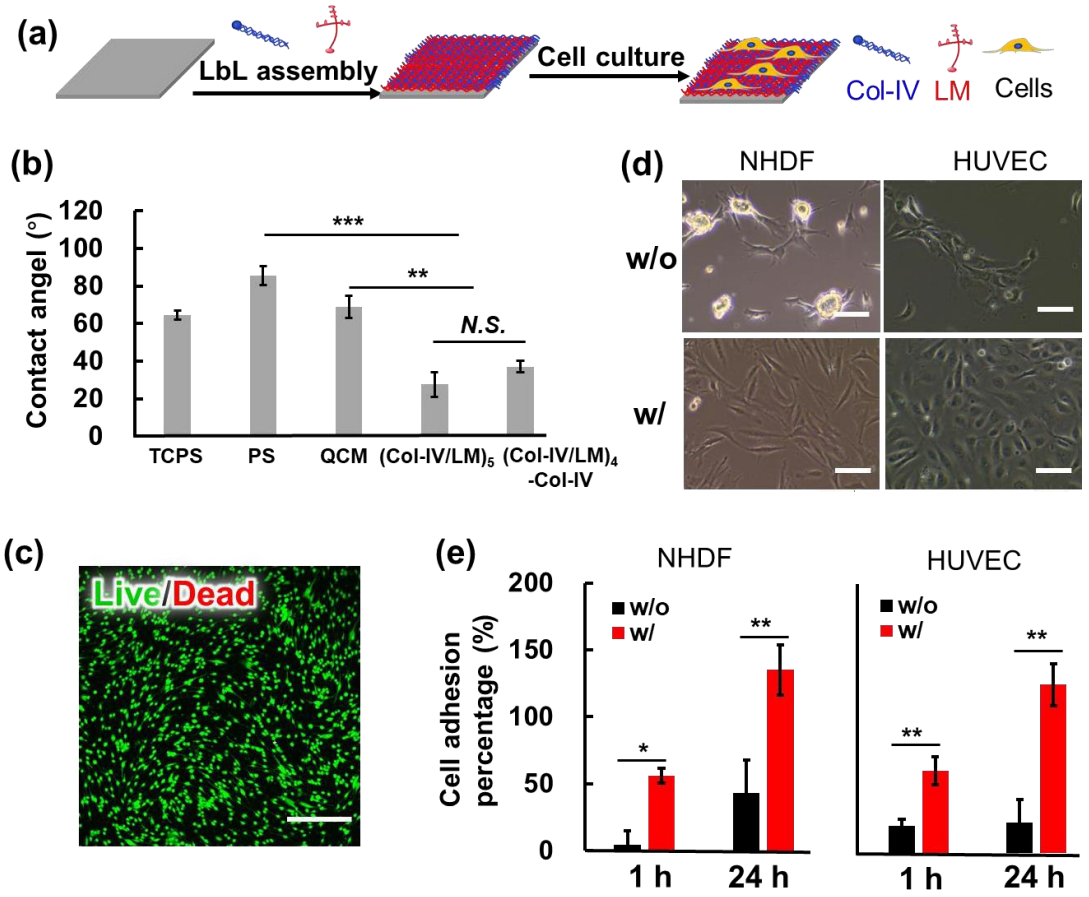

Figure 3. Cell adhesion on substrate coated with $(Col\text{-}IV/LM)_5$ nanofilms (26 nm). (a) Schematic image of LbL assembly process of Col-IV/LM nanofilms and cell adhesion on substrate. (b) Water contact angles measured on the surfaces of TCPS, PS, QCM chip, and QCM chips coated with $(Col\text{-}IV/LM)_5$ and $(Col\text{-}IV/LM)_4$-Col-IV nanofilms. n=3. (c) CLSM image of living cells stained by Calcein (green) and dead cells stained by Ethidium homodimer-1 (red). The scale bar is 300 μm. (d) Morphology of NHDF and HUVEC adhered onto PS substrate coated without (w/o) or with (w/) $(Col\text{-}IV/LM)_5$ nanofilms for 24 hours. Scale bars are 100 μm. (e) Percentage of NHDF and HUVEC adhered onto PS substrate without (w/o) or with (w/) $(Col\text{-}IV/LM)_5$ nanofilms after one- and 24-hours incubation. All data are representative of three independent experiments, mean±SD. *p<0.05, **p<0.01, ***p<0.001.

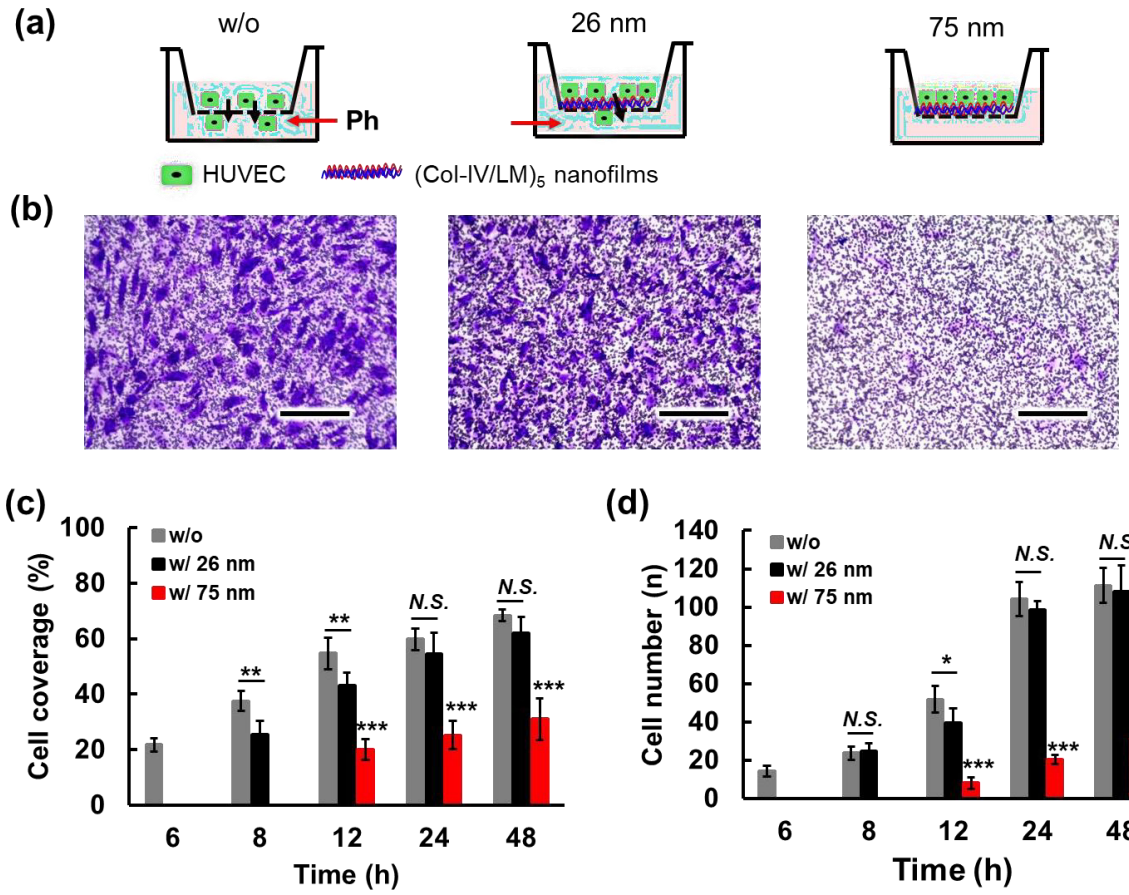

Figure 4. Barrier effect on HUVEC of (Col-IV/LM)5 nanofilms coated onto porous membranes (24-well insert with 3.0 μm pore size, 2.0×10^5 cells). (a) Schematic image of HUVEC migrated through the transwell membrane coated without (w/o) or with (w/) (Col-IV/LM)5 nanofilms. (b) Representative transwell images of crystal violet staining of migrated HUVEC through the transwell membrane coated without (w/o) or with (w/) (Col-IV/LM)5 nanofilms at 40 μg/mL and 1,000 μg/mL after incubation for 24 hours. Scale bars are 400 μm. (c) Migrated HUVEC coverage and (d) HUVEC number on the other side of the transwell membrane calculated by crystal violet staining in 1800×1350 μm. The data are representative of three independent experiments and five phase contrast microscopic images were counted, mean±SD, *p<0.05, **p<0.01, ***p<0.001.

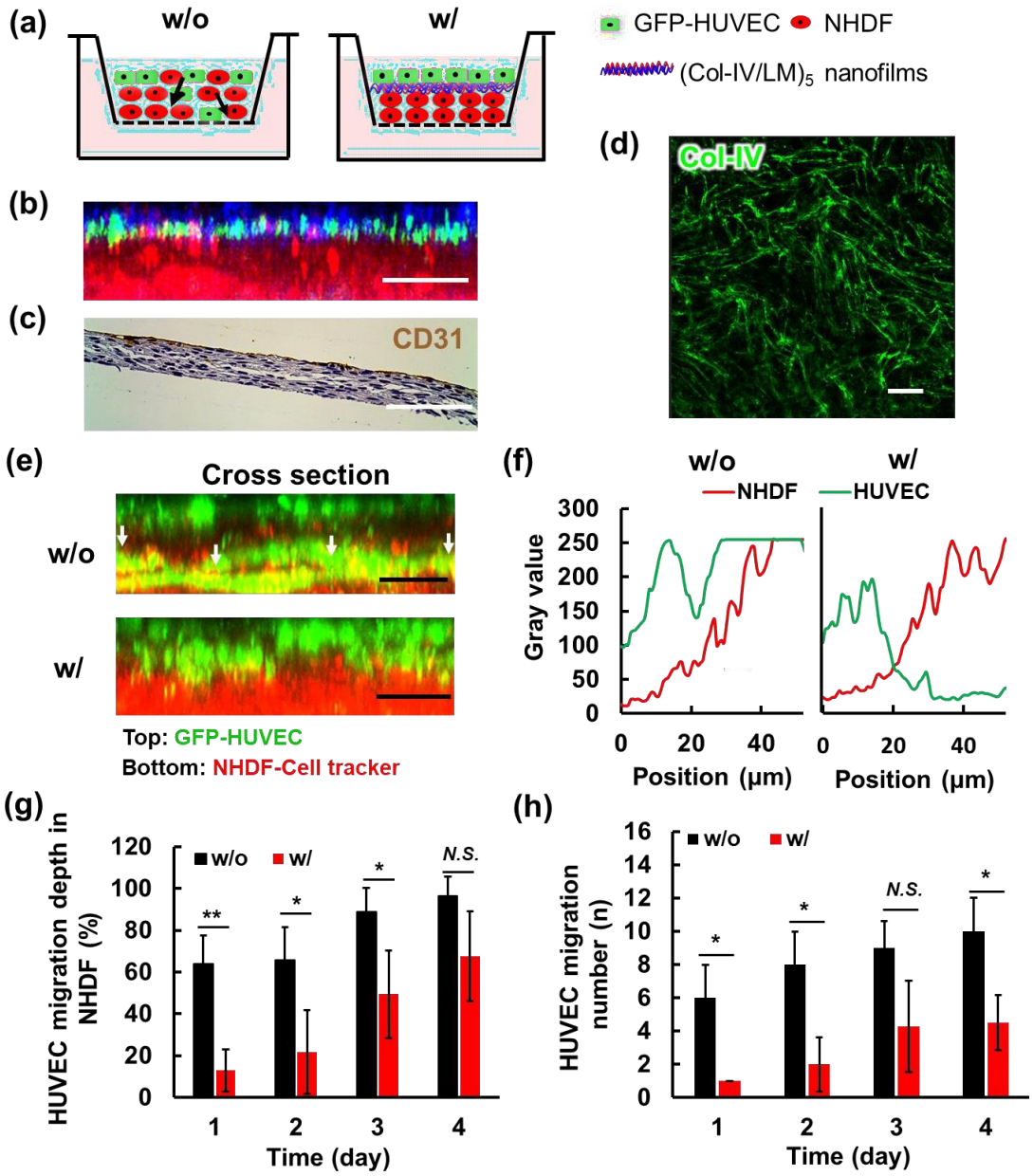

Figure 5. Barrier effect on HUVEC of (Col-IV/LM)5 nanofilms located between HUVEC monolayer and NHDF layers. (a) Schematic image of random cells co-culture without (Col-IV/LM)5 nanofilms and patterned cells co-culture with the barrier effect of (Col-IV/LM)5 nanofilms. (b) Cross-sectional CLSM image showing the distribution of $(Col\text{-}IV/LM)_5$ nanofilms (26 nm, FAM conjugated Col-IV in green) between the HUVEC monolayer (CD31 immunostained in blue) and NHDF layers (stained by Cell Tracker™ Deep Red). Scale bar is 30 μm. (c) Histological observation of a cross-sectioned compartmentalized cells co-culture (HUVEC were stained with CD31, toluidine staining for nuclei). Scale bar is 100 μm. (d) Fluorescence image of (Col-IV/LM)5 nanofilm morphology (FAM conjugated Col-IV in

green). The scale bar is 50 μm. (e) Cross-sectional CLSM images of the barrier prepared using (Col-IV/LM)5 nanofilms with 75 nm (1,000 μg/mL) show penetration of GFP-HUVEC through NHDF (stained by Cell Tracker™ Deep Red) layers and mixed layers on the bottom after 3 days incubation. Scale bars are 50 μm. (f) Linear scanning of gray value of two fluorescence intensity from top to bottom according to Figure 5e. (g) Percentage of HUVEC migration depth through NHDF layers without (w/o) or with (w/) (Col-IV/LM)5 nanofilms over a period of 4 days counted according to the CLSM images of 3D cell aggregation. Three CLSM images were counted, mean±SD. (h) Migrated HUVEC number through NHDF layers without (w/o) or with (w/) (Col-IV/LM)5 nanofilms over a period of 4 days were counted according to CLSM images of 3D cell aggregations. n=3. *$p<0.05$, **$p<0.01$, ***$p<0.001$.

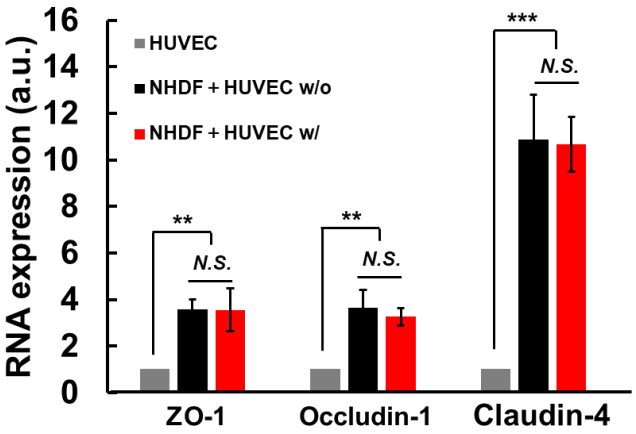

Figure 6. RT-qPCR analyze of tight juction proteins expression of HUVEC. Tight juction proteins expression of HUVEC co-cultured with NHDF, which are separated without (w/o) or with (w/) (Col-IV/LM)5 nanofilms (1,000 μg/mL) between HUVEC layers and NHDF layers, were compared with simple 2D HUVEC culture. The results were normalized by VE-cadherin gene expression. n=3, **p<0.01, ***p<0.001.

The table of contents

Nanometer-sized artificial basement membranes based on collagen type IV and laminin were prepared by a layer by layer assembly method. Multilayered nanofilms show similar fibrous structure, cell adhesion properties and barrier effects as natural basement membranes. Separation between fibroblast cells and endothelial cells will contribute to the construction of compartmentalized 3D tissues.

Fabrication of Artificial Nano-Basement Membranes for Cell Compartmentalization in 3D Tissues

J. Zeng, N. Sasaki, C. R. Correia, J. F. Mano and M. Matsusaki*

ToC figure